Mon. Not. R. Astron. Soc. **336,** 1293–1303 (2002)

An excess of submillimetre sources towards $z \sim 1$ clusters

P. N. Best★

Institute for Astronomy, Royal Observatory Edinburgh, Blackford Hill, Edinburgh EH9 3HJ

Accepted 2002 July 16. Received 2002 July 9; in original form 2002 January 9

ABSTRACT

Deep submillimetre (submm) observations using SCUBA are presented of the central regions of four high-redshift clusters which have been extensively studied optically: CL0023 + 0423 ($z = 0.84$), J0848 + 4453 ($z = 1.27$), CL1604 + 4304 ($z = 0.90$) and CL1604 + 4321 ($z = 0.92$). 10 submm sources are securely detected towards these four clusters at 850 μm, with two further tenuous detections; the raw 850-μm source counts exceed those determined from blank-field surveys by a factor ∼3–4. In particular, towards CL1604 + 4304, six sources are detected with $S_{850\mu m} > 4$ mJy making this the richest submm field discovered to date. Corrections for gravitational lensing by these high-redshift clusters reduce these excess sources counts, but are unlikely to account for more than about half of the excess, with the remainder presumably directly associated with cluster galaxies. The 450- to 850-μm flux density ratios of the detected sources are systematically higher (at a significance level >98 per cent) than those determined for blank-field selected sources, consistent with them being at the cluster redshifts. If subsequent identifications confirm cluster membership, these results will demonstrate that the optical Butcher–Oemler effect is also observed at submm wavelengths.

Key words: galaxies: clusters: general – galaxies: starburst – submillimetre.

1 INTRODUCTION

Our understanding of star formation at high redshift has undergone a revolution in recent years. Lyman-dropout techniques (e.g. Steidel et al. 1996) have identified thousands of high-redshift field galaxies with star formation rates of a few $M_\odot\ yr^{-1}$, providing estimates of the cosmic evolution of the mean global star formation rate (e.g. Madau, Pozzetti & Dickinson 1998). However, it has also become clear that dust plays a very important role in star-forming galaxies, absorbing a significant proportion of the emitted light.

In order to directly address the role of dust, several submm blank field surveys have been carried out using the Submillimetre Common-User Bolometer Array (SCUBA; Holland et al. 1999) on the James Clerk Maxwell Telescope (JCMT), to various depths and sky areas. These have provided number counts of submm sources down to below 1 mJy at 850 μm (Smail, Ivison & Blain 1997; Hughes et al. 1998; Barger, Cowie & Sanders 1999; Blain et al. 1999; Eales et al. 2000; Scott et al. 2002; Cowie, Barger & Kneib 2002), and have resolved the majority of the submm background radiation into ultraluminous galaxies with SFR $> 100\ M_\odot\ yr^{-1}$ (Blain et al. 1999). The host galaxies of these sources show high optical obscuration, and so are missed by ultraviolet selection techniques (cf. Adelberger & Steidel 2000). SCUBA observations pointed at Lyman-break galaxies have failed to detect the vast majority to a combined sample noise level of about 0.5 mJy, indicating that these galaxies do not contribute significantly to the submm background (e.g. Chapman et al. 2000). Using a statistical analysis, Peacock et al. (2000) demonstrated that Lyman-break galaxies are correlated with faint background fluctuations (at the ∼0.1 mJy level) in a deep SCUBA image of the *Hubble Deep Field*, and calculated that on average the true star formation rates of Lyman-break galaxies are about a factor of 6 higher than those determined from their measured ultraviolet luminosities. This is consistent with other determinations that the global star formation rate at high redshifts should be at least a factor of a few higher than that measured optically (e.g. Hughes et al. 1998).

The ultraviolet and submm selection techniques clearly sample different populations of star-forming galaxies, and so to obtain a complete census of star formation at high redshifts, observations of both normal and dusty galaxies are required. Whilst these have been carried out for the field, to date high-redshift cluster environments have been neglected at submm wavelengths.

Rich galaxy clusters contain large numbers of galaxies at the same distance, and so provide important testbeds for models of galaxy evolution. The cores of low-redshift clusters are dominated by a population of luminous early-type galaxies; the optical properties of these evolve only very slowly with redshift, in a manner consistent with passive evolution of stellar populations which formed at a very early cosmic epoch (e.g. van Dokkum et al. 1998a,b; Schade, Barrientos & Lopez-Cruz 1997; Ellis et al. 1997; Stanford et al. 1998). Low-redshift clusters have been targeted at submm wavelengths, using them as lenses to magnify the background population; only two cluster galaxies have been detected within seven

★E-mail: pnb@roe.ac.uk

clusters at redshifts $0.19 < z < 0.41$ (Edge et al. 1999; see also Chapman et al. 2002), and both of these were centre cluster galaxies hosting powerful radio sources, in clusters with strong cooling flows.

The composition of clusters is a strong function of redshift, however: Butcher & Oemler (1978) showed that at $z > 0.3$ a population of bluer galaxies appears in many, but not all, clusters (the Butcher–Oemler effect). These blue galaxies often exhibit strong Hα or [O II] 3727 emission lines, indicative of on-going star formation. (Dressler et al. 1997, 1999) High-redshift clusters also show an increased number of weak radio sources (e.g. Dwarakanath & Owen 1999; Morrison 1999; Smail et al. 1999; Best et al. 2002), whose presence is correlated with the Butcher–Oemler blue galaxy population, though without correspondence of the host galaxies. The host galaxies of these weak radio sources comprise a mixture of starbursts and AGN. This increase in activity in high-redshift clusters is not unexpected. Low-redshift clusters have the majority of their gas and galaxies in stable virialized orbits with the galaxies in the cluster centre having been stripped of gas (e.g. Gunn & Gott 1972), switching off star formation. High-redshift clusters, on the other hand, are much younger, still in their formation process with relatively high galaxy merger rates (e.g. van Dokkum et al. 1999) and a plentiful supply of disturbed gas, and thus provide ideal laboratories to induce both starbursts and AGN.

To fully understand galaxy and cluster evolution, it is important to investigate the on-going star formation in these high-z clusters using submm studies as well as the standard optical selection techniques. This paper presents the first results of a submm survey of the central regions of high-redshift clusters, designed to address this issue. The sample selection, observations and data reduction are described in Section 2. In Section 3 the four clusters are individually discussed. The nature of the detected submm sources, their likelihood of being cluster members, and their global properties are discussed in Section 4. Conclusions are drawn in Section 5. Values for the cosmological parameters of $\Omega_{\rm M} = 0.3$, $\Omega_\Lambda = 0.7$ and $H_0 = 65$ km s^{-1} Mpc^{-1} are adopted throughout.

2 OBSERVATIONS AND DATA REDUCTION

2.1 Details of the observations

Cluster targets were selected from the literature based upon the following criteria: (i) they should have redshifts $z > 0.8$; (ii) deep imaging of the field should have been carried out, confirming a large overdensity of red galaxies; (iii) there should exist detailed spectroscopic observations of the field, with at least 10 galaxies being spectroscopically confirmed as cluster members. These criteria should ensure that the cluster targets are indeed genuine high-redshift clusters. Four clusters were selected according to these criteria and observing time constraints: CL0023 + 0423 ($z = 0.84$), J0848 + 4453 ($z = 1.27$), CL1604 + 4304 ($z = 0.90$) and CL1604 + 4321 ($z = 0.92$). This sample of clusters is not intended to be complete, but should be representative.

The central regions of the four clusters were observed at 850 and 450 μm simultaneously using SCUBA (Holland et al. 1999) on the JCMT during a variety of nights between 2000 February and 2001 December. Details of the observations are provided in Table 1. The 850-μm observations cover an area of sky approximately 2.5 arcmin in diameter, and have an angular resolution of about 14 arcsec. At 450 μm the observed sky area is slightly smaller and the beamwidth is about 7.5 arcsec.

Observations were taken using the standard 'jiggle-mode,' whereby the secondary mirror is moved around 64-point hexagonal pattern, with 1 s at each position, in order to fully sample both the 450- and 850-μm image planes. The secondary mirror is chopped at 7 Hz between 'on-source' and 'off-source' locations, and the telescope is also nodded every 16 s so that the chop position is placed at the opposite side of the field; the field is therefore observed in an

Table 1. Details of the SCUBA observations. For each cluster the redshift and pointing centre are given, together with the observation dates. For each observation date, the total number of 64-pt jiggle pattern repeats (10 jiggle repeats corresponds to about 30 min observing) and average CSO Tau (at 225 GHz) are given.

Cluster	z	RA (J2000)	Dec (J2000)	Obs date (dd-mm-yyyy)	$N_{\rm int}$ (64-pt jigs)	$\tau_{\rm CSO}$
CL0023 + 0423	0.84	00 23 52.3	+04 22 54	25-10-2000	130	0.09
				27-09-2001	77	0.06
				30-09-2001	50	0.10
				15-11-2001	30	0.06
				08-12-2001	90	0.06
J0848 + 4453	1.27	08 48 34.6	+44 53 42	26-02-2000	90	0.07
				27-02-2000	78	0.07
				28-02-2000	70	0.05
CL1604 + 4304	0.90	16 04 25.1	+43 04 53	02-03-2000	65	0.05
				03-03-2000	90	0.04
				04-03-2000	96	0.06
				21-03-2000	70	0.04
				22-03-2000	70	0.03
CL1604 + 4321	0.92	16 04 31.5	+43 21 17	25-10-2000	20	0.09
				28-01-2001	70	0.05
				29-01-2001	20	0.05
				04-05-2001	40	0.08
				05-05-2001	50	0.07
				06-05-2001	35	0.08
				08-05-2001	30	0.08
				27-09-2001	61	0.06

on–off–off–on pattern. A single 64-point jiggle sequence takes 128 s (plus overheads) to complete.

For this program the chop throw was fixed to be 45 arcsec in an east–west direction. This short chop throw results in the 'off' beam positions often also being within the field of view; where this is the case, the sources will have associated negative counterparts of half intensity 45 arcsec east and west of the true source. In addition to the popular belief at that time that a short chop throw improved sky-subtraction (the results of Archibald et al. 2002 now indicate that this is not correct), these negative regions provide an independent measurement of the source, increasing the signal-to-noise ratios and source reliabilities. The expected source density is sufficiently low that these regions are unlikely to coincide with another source.

A blazar was observed approximately every hour throughout the observations, to correct the pointing of the telescope. The pointing measurements before and after each source observation were used to correct for any pointing shift during the observation. The sky opacities were monitored by regular skydip observations throughout the nights. Flux calibration was determined by observing at least one of the flux calibrators Mars, Uranus and CRL618 each night, using the same 45-arcsec chop-throw as the targets. It is estimated that the photometry at 850 μm is accurate to about 5–10 per cent; at 450 μm the photometric accuracy is worse (predominantly systematics), with variations up to about 25 per cent.

2.2 Data reduction and cleaning

The observations were reduced using the SCUBA software, SURF (Jenness & Lightfoot 1998). The reference measurements were subtracted from the signal beams and the bolometers were flat-fielded using the standard SCUBA flat-field. Where CSO Tau data was available and reliable (i.e. stable, and consistent with the skydips) throughout the night, the 850- and 450-μm opacities were calculated for each observation using the CSO Tau relations provided by (Archibald, Wagg & Jenness 2000): $\tau_{850} = 4.02(\tau_{\rm CSO} - 0.001)$ and $\tau_{450} = 26.2(\tau_{\rm CSO} - 0.014)$. Where this was not possible, opacities were calculated by interpolating between the values determined from the preceding and succeeding skydips. After extinction corrections were applied, noisy bolometers, noisy integrations and strong spikes in individual bolometers were rejected; this removed between 5 and 10 per cent of the data. The sky variations were removed by subtracting, for each bolometer at each time-step, the mean signal over all of the other bolometers excluding those which had significantly higher than average noise.

The calibrated data sets from the different observing nights were weighted according to their rms noise levels and combined to produce maps of each cluster. These maps contain negative sidelobes east and west of each detected source, as discussed in Section 2.1. To remove these and to improve the fidelity of the images, the maps were cleaned using a modified version of the CLEAN algorithm (Högbom 1974) commonly used in radio astronomy. In this method, first a normalized beam-map is created from observations of CRL618 with the same chop-throw. Then, the highest peak on the source map is found, and the beam-map scaled and subtracted at this position to remove 10 per cent of this peak flux (i.e. a loop gain of 0.1). This removes some of the positive detection of a source, and partially fills in its negative sidelobes. The highest peak is allowed to be either positive or negative: although negative values are unphysical, this is important otherwise overcleaning of the map can give rise to spurious features when only positive noise peaks and not negative ones are cleaned. This cleaning was repeated for a number (typically 50 to 100) of iterations, until the highest peak found was within 2.5σ of the sky rms noise.

Each residual map comprises sky noise plus sources fainter than the minimum cleaned flux density. The flux removed from this map consists of a set of delta functions around the original source peaks; these are then convolved with a Gaussian of the same resolution as the JCMT beam and added back on to the map. The combined maps were then smoothed slightly by convolving them with a Gaussian, to lower the resolution to 16.5 arcsec at 850 μm and 9.5 arcsec at 450 μm in order to enhance the detectability of faint sources. The 850- and 450-μm maps of the clusters so produced are displayed in Figs 1 to 4. Comparison with the initial raw maps confirms that the cleaning process has reduced the background rms of the maps by removing the negative sidelobes, but not given rise to any new sources.

2.3 Source extraction

Perhaps the most uncertain aspect of the analysis of sub-millimetre data is the determination of the believability of sources from the final map. This arises primarily because of the small number of bolometers across the field (37 for the long wavelength array): noisy (or flagged) bolometers therefore lead to regions of higher noise in the map and can give rise to spurious sources. Several steps have been taken to avoid this. First, all fields have been observed either close to transit or with some observations either side of transit so that the bolometers rotate around the field, thus minimizing the effects of any bad bolometers. Secondly, except for J0848 + 4453, all fields have been observed during at least two separate runs, with consequent different noisy bolometers and different sky coverage. Thirdly, these different observing periods have been used to test the repeatability of detection of plausible sources (see below). Fourthly, on two of the 850-μm maps (J0848 + 4453 at location 08 48 35.55, + 44 54 24.7, and CL1604 + 4321 at location 16 04 27.63, + 43 21 52.9) the removal of bad bolometer data has led to regions of significantly shorter exposure and hence higher noise which may give rise to spurious sources: a 25-arcsec diameter region has been masked around these two locations.

From the final cleaned maps, both the peak and the integrated flux densities of likely sources were determined, the latter being measured by summing the flux density inside an aperture of radius 15 (10) arcsec at 850 (450) μm. The peak flux density (in mJy beam^{-1}) should be equal to the integrated flux density of the source (in mJy) for an unresolved source, and for extended sources it provides a lower limit. In low signal-to-noise observations, however, the peak flux density can overestimate the true flux densities, and the integrated flux density usually provides a more accurate measure. Sources with both peak and integrated flux densities measured at greater than 3.5σ, where σ is the rms sky noise of the map, were considered possible detections. Although within the 8 maps there are negative regions which reach -4σ in peak flux density, in no case does a region reach -3.5σ in both peak and integrated flux, and so there are unlikely to be any false positive detections at this significance level.

For each field, the observations were then divided into two or three subsets; in the case of J0848 + 4453 this was done by separating the first half of each night from the second half (i.e. by bolometer location on the map), and in the other three cases the separation was made by observing date. Independent maps were made for each subset of data. These maps were then examined to investigate the reliability of the sources detected above. All of the sources detected

Table 2. The SCUBA sources detected from the maps, at each of 850 and 450 μm. For each cluster the map rms noise is provided (note that the maps have been smoothed), together with a listing of the RA, Dec, offset from the cluster centre, peak flux density, and integrated flux density of each source. Statistical errors on the flux densities of individual sources are the rms of the sky background for the peak flux densities and approximately 1.5 times this value for the integrated flux densities. In addition there are associated calibration uncertainties for each map, at a level of 5–10 per cent at 850 μm and up to 25 per cent at 450 μm. The penultimate column of the table indicates for each source whether the detection is fully secure: sources which are detected above 4σ in integrated flux density are considered secure, whilst sources between 3.5 and 4σ are less so. The 3.9σ 850-μm source towards CL1604 + 4304 is also classified as secure because it is detected at 450 μm. The final column gives the 450/850 μm flux density ratio (or upper limit) for 850-μm sources with secure detections which lie within the 450-μm field of view.

Cluster	Array	Map rms [mJy bm^{-1}]	Source	RA (J2000)	Dec (J2000)	Offset [arcsec]	$S_{\rm peak}$ [mJy bm^{-1}]	$S_{\rm int}$ [mJy]	Secure?	S_{450}/S_{850} ratio
CL0023 + 0423	850 μm	1.2	HzCl0023_850.1	00 23 54.70	04 23 02.0	37	6.6	7.4	Y	$\lesssim 5.4$
			HzCl0023_850.2	00 23 53.66	04 21 55.6	62	5.6	4.7	?	
	450 μm	9.9	–	–	–	–	–	–		
J0848 + 4453	850 μm	1.6	HzCl0848_850.1	08 48 40.38	44 54 21.0	73	13.2	13.1	Y	
			HzCl0848_850.2	08 48 31.78	44 53 45.0	30	7.2	7.7	Y	$\lesssim 6.3$
	450 μm	12.2	–	–	–	–	–	–		
CL1604 + 4304	850 μm	1.1	HzCl1604a_850.1	16 04 23.93	43 04 35.5	22	8.5	9.4	Y	4.6 ± 1.4
			HzCl1604a_850.2	16 04 30.38	43 04 37.8	60	7.3	6.4	Y	$\lesssim 3.4$
			HzCl1604a_850.3	16 04 22.82	43 05 12.1	31	5.9	5.6	Y	5.4 ± 2.0
			HzCl1604a_850.4	16 04 23.63	43 05 27.8	38	5.5	5.4	Y	$\lesssim 4.1$
			HzCl1604a_850.5	16 04 24.28	43 03 52.0	62	5.2	4.6	Y	$\lesssim 4.8$
			HzCl1604a_850.6	16 04 26.38	43 03 55.0	60	3.9	4.3	Y	7.0 ± 2.8
	450 μm	5.5	HzCl1604a_450.1	16 04 23.80	43 04 38.1	21	36.3	43.6	Y	
			HzCl1604a_450.2	16 04 22.92	43 05 07.4	28	29.9	30.2	Y	
			HzCl1604a_450.3	16 04 26.41	43 03 56.9	58	30.0	30.1	Y	
			HzCl1604a_450.4	16 04 22.62	43 05 37.9	53	27.6	19.1	?	
CL1604 + 4321	850 μm	1.2	HzCl1604b_850.1	16 04 35.63	43 21 10.6	46	6.3	6.4	Y	7.4 ± 2.9
			HzCl1604b_850.2	16 04 33.33	43 22 32.0	77	6.4	4.2	?	
	450 μm	11.1	HzCl1604b_450.1	16 04 35.72	43 21 12.8	46	48.4	47.4	Y	

above 4σ in the overall map were also present above $\sim 2\sigma$ in each of the data subsets.

The detected sources are listed in Table 2. The reliability of each source is also indicated in the table: those sources which are detected above 4σ in integrated flux density are considered secure, whilst sources between 3.5 and 4σ are less so.

3 DISCUSSION OF INDIVIDUAL SOURCES

CL0023 + 0423

This cluster was discovered optically and appears in the cluster sample of Gunn, Hoessel & Oke (1986). It forms part of the sample of nine high-redshift clusters which Oke, Postman & Lubin (1998) have studied in detail with deep multi-waveband imaging and spectroscopic observations. Postman, Lubin & Oke (1998) show that the optical overdensity is actually the superposition of a cluster at $z = 0.845$, with a velocity dispersion of 415 km s^{-1} (corresponding to a dynamical mass $M \sim 3 \times 10^{14}$ M$_\odot$) and 17 spectroscopically confirmed galaxy members to date, and a group of lower velocity dispersion ($\sigma \sim 158$ km s^{-1}) at $z = 0.827$, with seven spectroscopically confirmed galaxies. These two structures are separated by less than 3000 km s^{-1} in redshift space, and may be interacting: about 57 per cent of the cluster members show evidence for star formation activity (Postman et al. 1998).

The 850-μm SCUBA image of this cluster (Fig. 1) shows one source of 7.4-mJy integrated flux density (HzCl0023_850.1), which appears significantly extended; this source appears in all subsets of the data, although with positional offsets of up to 5 arcsec, presumably because of the extended nature of the source. A second source (HzCl0023_850.2) is detected above 4σ in peak flux, but below 4σ in integrated flux, and so this is considered a marginal detection. No believable sources are detected at 450 μm.

J0848 + 4453

This cluster, the highest redshift in the current sample, was first discovered by Stanford et al. (1997) as a concentrated overdensity of very red objects in a near-infrared field survey. There is a 4.5σ significance X-ray detection ($L_{\rm X} \sim 10^{44}$ erg s^{-1}, 0.5–2 keV) at the same location. Follow-up spectroscopy has, to date, confirmed 10 galaxies as cluster members, with a velocity dispersion of 640 km s^{-1} suggesting a cluster of about Abell richness class 1 (Stanford et al. 1997). More recently, a second group of galaxies has been detected only 4 arcmin away, with redshift 1.26 (Rosati et al. 1999). This group also has associated X-ray emission of similar luminosity, and spectroscopic redshifts have confirmed cluster membership for six galaxies to date. The J0848 + 4453 cluster therefore appears to be part of a massive high-redshift structure.

The SCUBA maps of the central regions of this cluster indicate the presence of two luminous submm sources at 850 μm (see Fig. 2; Table 2). A slightly extended source is seen to the west of centre of the map (HzCl0848_850.2), and a very luminous (>13 mJy) source close to the north-eastern edge (HzCl0848_850.1). This latter source is amongst the most luminous 850 μm sources known; although it lies close to the edge of the field, it occurs in all subsets of the data and so its detection is considered secure.

CL1604 + 4304

Like CL0023 + 0423, the cluster CL1604 + 4304 ($z = 0.90$) was first discovered in the optical imaging search of Gunn et al. (1986)

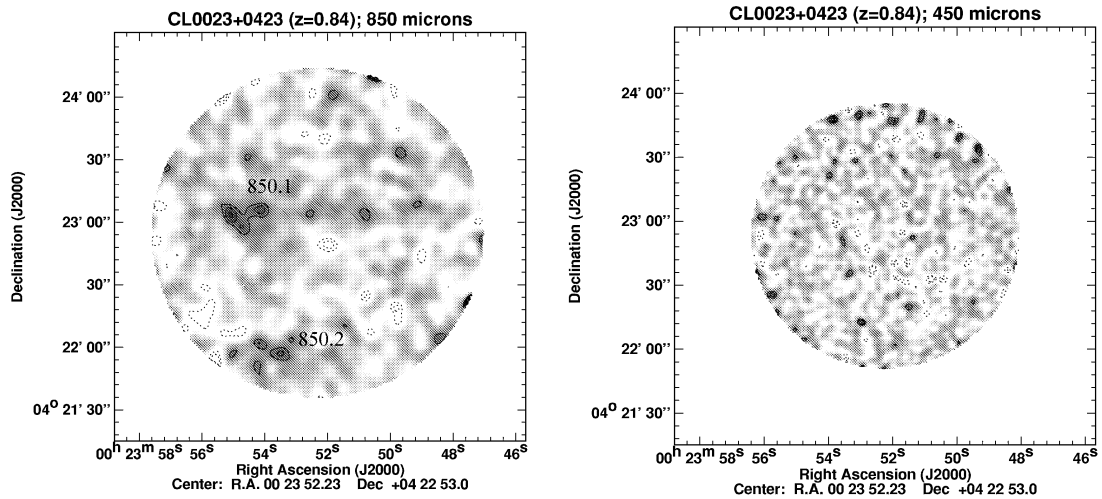

Figure 1. SCUBA maps at 850 and 450 μm of the central regions of the CL0023 + 0423 cluster at redshift $z = 0.84$. Contour levels are plotted at (−4, −3, 3, 4, 5, 6, 7, 8) times the sky rms noise level of each map: the 850- and 450-μm maps have rms noise levels of 1.2 mJy beam^{-1} and 9.9 mJy beam^{-1} respectively (note that the maps have been smoothed).

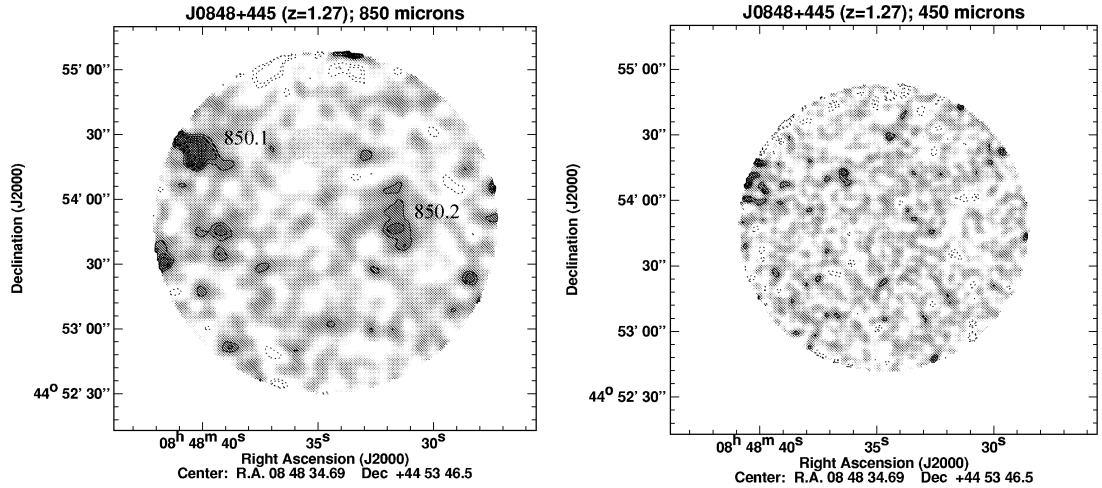

Figure 2. SCUBA maps at 850 and 450 μm of the central regions of the J0848 + 4453 cluster at redshift $z = 1.27$. Contour levels are plotted at (−4, −3, 3, 4, 5, 6, 7, 8) times the sky rms noise level of each map: the 850- and 450-μm maps have rms noise levels of 1.6 mJy beam^{-1} and 12.2 mJy beam^{-1} respectively (note that the maps have been smoothed). A 25 arcsec diameter region centred on 08 48 35.55, + 44 54 24.7 has been masked in the 850-μm map owing to a higher noise level associated with bolometer flagging.

and subsequently formed part of the sample of nine high-redshift clusters studied by Oke et al. (1998). This cluster was studied in considerable detail by Postman et al. (1998) and Postman, Lubin & Oke (2001): spectroscopic redshifts have been obtained for over a hundred galaxies in the field, with 22 being confirmed cluster members. The velocity dispersion of these galaxies, $\sigma \sim 1220$ km s^{-1}, is consistent with an Abell 2 richness cluster although the cluster is only marginally detected in X-rays with a luminosity of $\sim 10^{44}$ erg s^{-1} (0.1 to 2.4 keV; Castander et al. 1994), and Smail, Ellis & Fitchett (1994) failed to detect a weak lensing signal towards it. Approximately half of the confirmed cluster galaxies are emission line (star forming) objects.

This cluster is particularly interesting as it forms part of one of the most massive structures known at high redshifts. The equally rich cluster CL1604 + 4321 (also in the SCUBA sample: see below) is offset only 17 arcmin on the sky and 4300 km s^{-1} in redshift, and there is a large overdensity of red galaxies in a 'filament' joining the two clusters, including another smaller condensation of red galaxies (Lubin et al. 2000). Together these seem to comprise a very massive high-redshift supercluster.

The 850-μm SCUBA map of the central regions of this cluster is quite remarkable (Fig. 3). This is both the deepest map in the sample, and the one taken in the best, most stable, sky conditions and therefore of high image integrity. Five sources are clearly and securely detected with flux densities in excess of 4.4 mJy (4σ; see Table 2). A sixth source (HzCl1604a_850.6) is detected slightly below 4σ significance, but appears as a luminous source in the 450-μm observations (HzCl1604a_450.3), confirming its reality. A further two of the 850-μm sources are also detected at 450 μm, providing still further confirmation of their reality. A fourth 450-μm source is marginally detected at between 3.5 and 4σ, but the disparity between its peak and integrated flux densities and its non-detection at 850 μm cast doubt on its reality. The rms of the 450-μJy map is significantly lower than those of the

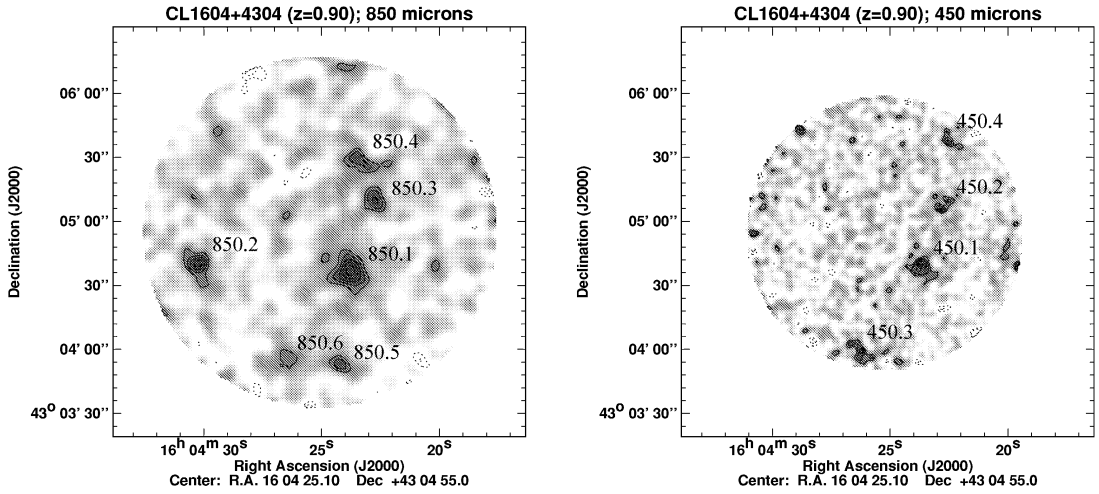

Figure 3. SCUBA maps at 850 and 450 μm of the central regions of the CL1604 + 4304 cluster at redshift $z = 0.90$. Contour levels are plotted at (−4, −3, 3, 4, 5, 6, 7, 8) times the sky rms noise level of each map: the 850- and 450-μm maps have rms noise levels of 1.1 mJy beam^{-1} and 5.5 mJy beam^{-1} respectively (note that the maps have been smoothed).

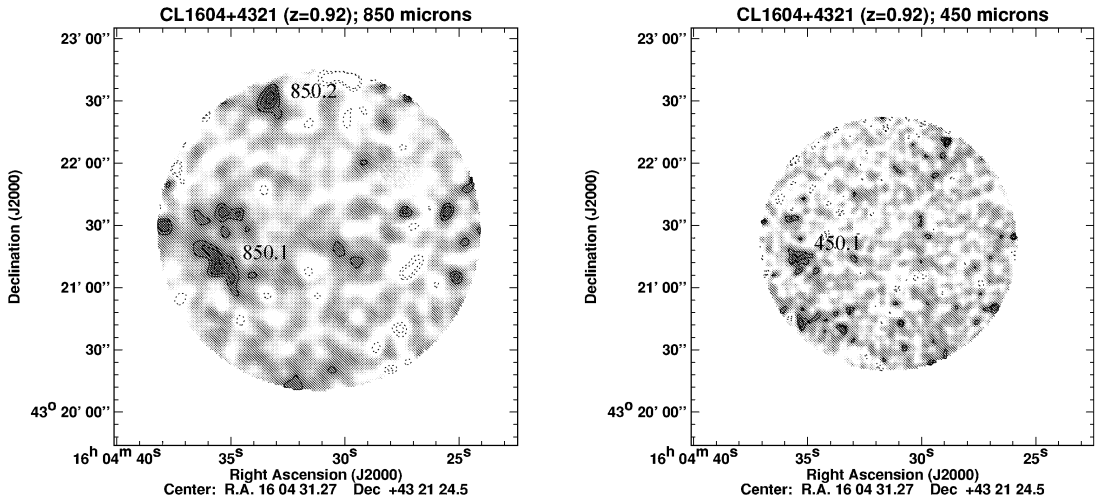

Figure 4. SCUBA maps at 850 and 450 μm of the central regions of the CL1604 + 4321 cluster at redshift $z = 0.92$. Contour levels are plotted at (−4, −3, 3, 4, 5, 6, 7, 8) times the sky rms noise level of each map: the 850- and 450-μm maps have rms noise levels of 1.2 mJy beam^{-1} and 11.1 mJy beam^{-1} respectively (note that the maps have been smoothed). A 25 arcsec diameter region centred on 16 04 27.63, +43 21 52.9 has been masked in the 850-μm map due to a higher noise level associated with bolometer flagging.

other clusters in the sample due to the low opacities during these observations.

The detection of six sources brighter than 4 mJy at 850 μm makes this the richest submm field observed to date. The source density on this map is a factor of 5 higher than expected from blank field counts (see Section 4.1).

CL1604 + 4321

As discussed above, CL1604 + 4321 at redshift 0.92 forms part of a potential high-redshift supercluster together with CL1604 + 4304. Postman et al. (2001) studied CL1604 + 4321 in detail, and spectroscopically confirmed about 40 galaxies as being associated with the cluster, with a velocity dispersion of 935 km s^{-1}.

One source is clearly detected above the 4σ level at both 850 and 450 μm in the SCUBA maps (HzCl1604b_850.1 and 450.1; Fig. 4; Table 2). A second source, towards the north-east edge of the 850-μm map, is detected with an integrated flux density level between 3.5 and 4σ, and so is considered to be an insecure detection.

4 RESULTS

10 submm sources have been securely detected towards these four high-redshift clusters at 850 μm, with a further two possible detections. The important issue is now to determine whether these sources are indeed associated with the clusters or whether they are merely projected along the same line of sight. Before all of the sources are identified and their redshifts measured, this question cannot be unambiguously answered, but in this section some indications are given based upon the source counts and upon the 450/850 μm flux density ratio which serves as a rough redshift indicator.

4.1 Integrated source counts

The integrated source counts at 850 and 450 μm have been determined as a function of limiting flux density using the integrated

flux densities of each source. Scott et al. (2002) found, using simulated maps, that the flux densities of sources in the 8-mJy survey are typically overestimated due the effects of both noise and source confusion; here no corrections were made for this effect, because our sky area covered is too small and contains too many sources to accurately calculate any such corrections. At the significance levels ($>4\sigma$) of the sources considered, the flux boosting effects due to noise should be minimal, and in any case any such flux boosting is compensated by the fact that the 15 arcsec radius aperture will not contain the total source flux density – in theory only ∼95 per cent for a point source. Confusion effects, however, could be important if faint sources below the flux limit combine to give an apparent source above that limit. One or two of the more extended sources could conceivably be the result of source confusion, although the simulations of Hughes & Gaztañaga (2000) suggest that this effect is of little importance at flux densities above ∼2.5 mJy, and so from here on it is discounted.

Only the securely detected sources were considered in this analysis. At 850 μm the sky area observed in each map was taken to be 4.5 arcmin^2 down to a flux density level of 4 times the rms noise quoted in Table 2, plus a further 1 arcmin^2 around the edges of the map to a flux density level 50 per cent higher. At 450 μm the sky areas were similarly 3 arcmin^2 at the highest sensitivity and 1 arcmin^2 at the lower sensitivity. Between each of the eight limiting flux densities (that is, the limiting values for the central and edge regions of each map), the sky area sampled brighter than this limit was determine and used to calculate the number density of sources within that flux density range. From these were calculated the number density of sources above three flux density levels at 850 μm and a single level at 450 μm. These are provided in Table 3. It is important to note that at this stage no account is taken of any possible gravitational lensing by the clusters, and so the raw source counts likely overestimate the true counts; this is discussed in detail in Section 4.2.

The integrated source counts determined at 850 μm are compared with those determined from blank field surveys on Fig. 5. The comparison data are taken from the *Hubble Deep Field* survey (Hughes et al. 1998), the various SCUBA lensing surveys – after correction for lensing amplification – (Smail et al. 1997; Blain et al. 1999; Cowie et al. 2002), the Hawaii Survey Fields (Barger et al. 1999), the Canada–UK Deep Submillimetre Survey (Eales et al. 2000) and the 8-mJy Survey (Scott et al. 2002). Fig. 5 shows that the 850-μm counts towards the high-redshift clusters are clearly in excess, by a factor ∼3–4, of those in the blank field surveys. Note that a similar excess of 850-μm counts has also been found in the field surrounding the high-redshift ($z = 3.8$) radio galaxy 4C14.17, which is thought to reflect a high-redshift proto-cluster (Ivison et al. 2000a). It should be noted that the sky areas sampled are relatively small, and SCUBA sources are known to be highly clustered (Scott et al. 2002; Almaini et al. 2002), which could give rise to higher

Table 3. The integrated source counts as a function of limiting flux density at 850 and 450 μm as observed in the fields of the high-redshift clusters.

Wavelength [μm]	Flux density [mJy]	N(>S) [deg^{-2}]	ΔN [deg^{-2}]
850	7.2	680	340
	6.0	1150	470
	4.3	3300	1000
450	25.0	3800	1900

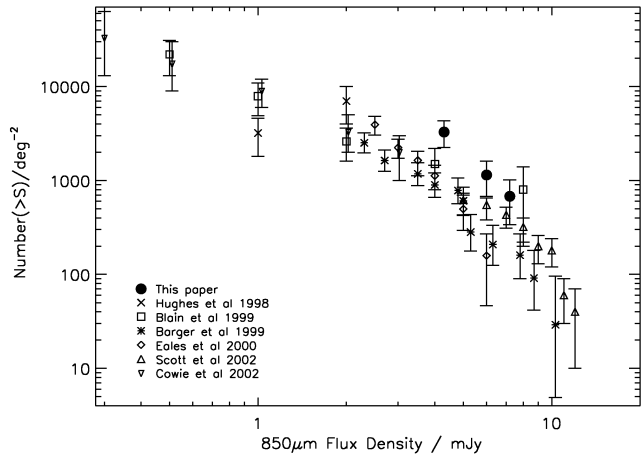

Figure 5. The integrated source counts at 850 μm as observed in the fields of the high-redshift clusters (filled circles) compared with those determined from various SCUBA field surveys (open symbols), taken from the references indicated in the lower left corner of the plot (the results from the lensing surveys have been corrected for amplification). A clear excess of submm galaxies is seen in the direction of the high-redshift clusters.

than average counts being measured in some locations. Although this possibility cannot be definitively excluded until identifications and redshifts are available for the sources, for such a strong overdensity to occur by chance just at the location of these clusters would be an odd coincidence, and so it is far more likely that the excess is real (or due to lensing; see below).

At 450 μm determining the source counts is considerably more uncertain due to the fewer sources detected and the larger uncertainties in calibration. Smail et al. (2002) derive 450 μm source counts to be 2100 ± 1200 deg^{-2} sources brighter than 10 mJy and 500 ± 500 deg^{-2} sources brighter than 25 mJy. The 3800 ± 1900 counts deg^{-2} determined here to the same 25-mJy flux density limit is almost an order of magnitude in excess of their counts, although the errors are clearly large.

4.2 Gravitational lensing?

Because these sources are observed in directions towards concentrations of mass, the possibility of gravitational lensing by the high-redshift clusters must be considered. Gravitational lensing has two competing effects upon the observed distribution of source counts: the apparent luminosity of each lensed source is increased, boosting the apparent source counts, but the sky area observed is decreased in the lensed regions.

Prior to any lensing the total source counts observed will be $N(S_\nu) = \int_0^{z_{\max}} n(S_\nu, z)\,\mathrm{d}z$, where $n(S_\nu, z)$ describes the source counts as a function of redshift. After lensing by a factor $\mu(\theta, z)$, where θ is the angular offset from the lens centre, the observed source counts will be

$$N'(S_\nu, \theta) = \int_0^{z_{\max}} \frac{1}{\mu(\theta)} n\left[\frac{S_\nu}{\mu(\theta)}, z\right] \mathrm{d}z.$$

If the source counts can be described by a power law, $n(S_\nu, z) \propto S_\nu^{-\alpha}$, then $n(S_\nu/\mu, z) = \mu^\alpha n(S_\nu, z)$ and therefore $N'(S_\nu, \theta) = \mu(\theta)^{\alpha-1} N(S_\nu)$. When the slope ($\alpha$) of the power-law exceeds unity then the effects of gravitational lensing can boost the observed source counts. Fig. 5 demonstrates that the submm source counts indeed have a very steep slope: the slope of the integrated source counts, $N(>S_\nu)$, is about 1.8, and so $\alpha \sim 2.8$. Thus a magnification

of a factor 2 provides a boost in the source counts of approximately a factor 3.5. It is this dramatic effect which has led to low-redshift rich clusters being used as lenses to study the faint submm source population (e.g. Smail et al. 1997).

Modelling the lensing object as a singular isothermal sphere (SIS), that is, one with a central density profile of $\rho(r) \propto r^{-2}$, the factor by which the sources are magnified at an angular offset θ is related to the Einstein radius, $\theta_{\rm E}$, by:

$$\mu(\theta) = \left| 1 - \frac{\theta_{\rm E}}{\theta} \right|^{-1}.$$

The Einstein radius can be expressed in terms of the properties of the source and lens as (e.g. Blandford & Narayan 1992):

$$\theta_{\rm E} = \frac{4\pi\sigma^2}{c^2} \frac{D_{\rm LS}}{D_{\rm OS}},$$

where σ is the velocity dispersion of the lens, $D_{\rm LS}$ is the angular distance between the source and lens, and $D_{\rm OS}$ is the angular distance between the source and the observer. The lensing magnification is maximal for sources observed at the Einstein radius (theoretically infinite for a point source, and in practice giving rise to strongly-lensed arcs or multiple images) but falls off rapidly beyond this: at $\theta = 2\theta_{\rm E}$ the magnification factor $\mu(\theta) \sim 2$, and by $4\theta_{\rm E}$ it is only a factor of 1.33. For flatter central density profiles, for example the NFW profile (Navarro, Frenk & White 1997) with $\rho(r) \propto r^{-1}$, the magnification factors beyond $\theta_{\rm E}$ are lower than for the SIS.

The velocity dispersions of the four clusters in this sample are very uncertain because of the small numbers of redshifts currently available. The estimated values range from 415 to 1220 km s^{-1} for the four clusters (Rosati et al. 1999; Postman et al. 2001). Adopting a velocity dispersion of 1000 km s^{-1}, a lens redshift $z_{\rm L} = 1$ and a source redshift $z_{\rm S} = 3$, the Einstein radius corresponds to $\theta_{\rm E} \sim 13$ arcsec. This value is significantly smaller than for low-redshift rich clusters (up to 30 or 40 arcsec), first because the high-redshift clusters are of significantly lower mass (velocity dispersion) and secondly because the optimal lensing configuration has equal source-lens and lens-observer distances which favours $0.2 \lesssim z_{\rm L} \lesssim 0.4$ for $2 \lesssim z_{\rm S} \lesssim 4$. Therefore the effects of magnification by these high-redshift clusters are of lesser importance unless the SCUBA population are at $z_{\rm S} \gg 5$.

A proper determination of the unlensed source counts cannot be carried out without an accurate mass model for these clusters, but a rough judgement of the importance of lensing magnification can be made. Integrating the expression for the magnified source counts across the field using an Einstein radius of 13 arcsec ($\sigma \sim 1000$ km s^{-1}) predicts a total boosting of the 850-μm source counts of a factor between 1.5 and 2 for an SIS profile. This is consistent with the boosting in number counts that might be expected by examining the distribution of detected sources within the fields: the offsets of each individual source from the cluster centre are given in Table 2. HzCl1604a_850.1 has a angular offset from the cluster centre of only ∼20 arcsec indicating that it is likely to be significantly magnified; the relatively low 450- to 850-μm flux density ratio of this source (see Section 4.3) further supports the suggestion that this is a background source. Four further objects (HzCl0023_850.1, HzCl0848_850.2, HzCl1604a_850.3 and HzCl1604a_850.4) have angular offsets of between 30 and 40 arcsec, with consequent flux boosting of ∼50 per cent if these are lensed background objects, but all of the remaining seven sources are more than 40 arcsec away from their cluster centres, with expected flux boostings of $\lesssim$25 per cent. The radial distance of all but one sources is at least double the Einstein radius, making it extremely unlikely that any multiple image strong lensing affects the number counts in these clusters.

It should be stressed that, unless the current velocity dispersion measurements greatly underestimate the mass of these clusters, these calculations represent the upper limit of the boosting that gravitational lensing by the cluster could feasibly provide. The $\sigma \sim 1000$ km s^{-1} adopted is very much at the maximum for clusters at these redshifts, and the SIS profile represents the 'worst-case' scenario. Further, for CL1604 + 4304 with the most detected submm sources and the highest estimated velocity dispersion, not even a weak-lensing signal was seen for optical galaxies in the analysis of Smail et al. (1994). Therefore although cluster gravitational lensing is likely to have a significant effect upon the source counts, this is not nearly to the extent of the factor ∼3.5 higher source counts that is observed.

An alternative factor that could conceivable boost the source counts is gravitational lensing by individual galaxies. It was suggested a few years ago that the brightest SCUBA source in the *Hubble Deep Field* is gravitationally lensed by a $z \sim 1$ elliptical (Downes et al. 1999), and indeed Dunlop et al. (2002) have recently shown this to be the case, with of order a factor of 3 boosting of the submm flux density of this source. Within a $z \sim 1$ cluster there is a higher surface density of elliptical galaxies which could act as lenses. The Einstein radius of an individual elliptical galaxy at these redshifts will be only $\theta_{\rm E} \sim 1$–2 arcsec; an examination of optical data available for CL1604 + 4304 (Smail et al. 1994) suggests that the SCUBA source lies this close to a bright elliptical in only one of the six cases, that being HzCl1604a_850.1 which was already suggested to suffer strong cluster lensing. Once again, therefore, this effect is unlikely to significantly affect the number count statistics, but could be relevant in isolated individual cases. This is an important effect to bear in mind during follow-up studies as it can easily lead to misidentification of the host galaxy (cf. Downes et al. 1999).

All in all, the conclusion must be (particularly when coupled with the redshift indicators below) that the higher source counts are in part due to lensing effects, both from the cluster and individual galaxies, but that a significant population of cluster sources is also detected.

4.3 Redshift indicators

Identifying the host galaxies of submm sources and measuring their redshifts spectroscopically is notoriously difficult, (e.g. Dunlop et al. 2002) and so photometric redshift indicators are required. Various redshift indicators have been used, including submm flux density ratios, radio to submm spectral indices, millimetre or mid-IR data, or optical to near-IR colours (e.g. Carilli & Yun 2000; Ivison et al. 2000b; Smail et al. 2002; Chapman et al. 2002; Dunlop et al. 2002).

The most readily available redshift estimator is the 450- to 850-μm flux density ratio. For a dust temperature of 30 to 50K, the grey-body dust spectral energy distribution (SED) peaks at ∼100 μm. Thus, whilst the 850-μm data point lies on the Rayleigh-Jeans tail, providing a strong positive K-correction which results in the 850-μm flux density of a given source appearing the same at all redshifts $1 \lesssim z \lesssim 5$–10 (e.g. Blain & Longair 1993), the 450-μm data point moves steadily through the peak of the SED with increasing redshift. The 450- to 850-μm flux density ratio therefore decreases monotonically with redshift, providing a broad redshift estimator. In practice, since 450-μm calibration is notoriously difficult except in the best atmospheric conditions (such as those for the observations of CL1604 + 4304), calibration errors lead to systematic offsets and using the 450- to 850-μm flux density ratio provides uncertain results. Other redshift estimators are generally better, and in addition

the accurate positions determined from, for example, millimetre or radio data, allow optical identifications to be made. Radio observations of these fields are proceeding and will provide more definitive results in the future, but with the current data the 450- to 850-μm flux density ratio can provide some good first indications.

Lutz et al. (2001) investigated the how the 450- to 850-μm flux density ratio would vary as a function of redshift from the spectral energy distributions of 14 local ultra-luminous infrared galaxies (ULIRGs) with existing far-infrared and submm photometry (from Klaas et al. 2001). The relation they derived is shown in Fig. 6(a). 450- to 850-μm flux density ratios were calculated for all of the securely detected 850-μm sources in the current sample within the sky area of the 450-μm maps. These ratios are tabulated in Table 2 and are displayed as a histogram in Fig. 6(b). For four sources a flux density ratio is determined, for 3 of which the ratio is high, $\gtrsim$5, consistent with being at redshifts $z \lesssim 1$. A further four sources have determined upper limits on their flux ratios, which in three cases suggest relatively high redshifts when compared directly to the predictions of Fig. 6(a), although the presence of any cooler ($T \sim 10$–15 K) dust components within the galaxies would give rise to lower 450- to 850-μm flux density ratios at lower redshifts.

In Fig. 6(c) a similar histogram of flux density ratios has been derived for sources detected in blank field surveys, using the 8-mJy survey (Scott et al. 2002; Fox et al. 2002) and the SCUBA lensing survey (e.g. Smail et al. 1997, 2002); these provide a good spread of sources both more and less luminous than those of the high-redshift cluster sample, and so provide a good comparison sample. This figure provides a strong visual indication that the sources in the current sample have systematically higher 450- to 850-μm flux density ratios than those in the blank field surveys, for example considering the fraction of sources with 450- to 850-μm flux density ratios above and below 4.0 in each sample. Survival analysis (e.g. Feigelson & Nelson 1985) can be used to statistically investigate data sets such as these with large numbers of upper limits. The Kaplan–Meier estimator gives a mean 450- to 850-μm flux density ratio for the blank field selected sources of 3.0 ± 0.2 and even if all of the 5 upper limits for the cluster sample are between 2.0 and 2.5[1] then the mean for that sample will be $\gtrsim$4. Using the ASURV survival analysis package (LaValley, Isobe & Feigelson 1992) the likelihood of the sources from the cluster and blank field surveys being drawn from the same parent population, as determined from the 450- to 850-μm flux density ratio distributions, was calculated according to 5 different survival analysis methods based around a generalized Wilcoxin test: taking the mean of these results, the probability of the parent samples being the same is $\lesssim$1.8 per cent.

To summarize, the 450- to 850-μm flux density ratios of the current sample are systematically higher than those of blank field surveys. This is most likely due to an extra population of sources associated with the high-redshift clusters, which have higher 450- to 850-μm flux because their redshifts are significantly lower ($z \sim 1$) than sources typically detected in blank field surveys ($z \gtrsim 2$; e.g. Smail et al. 2000).

4.4 Dust masses and star-formation rates

The mass of warm dust, $M_{\rm d}$, can be calculated from the submillimetre flux using the equation:

[1]The Kaplan–Meier estimator cannot be applied to the cluster sample since the lowest data point is an upper limit rather than a measured value.

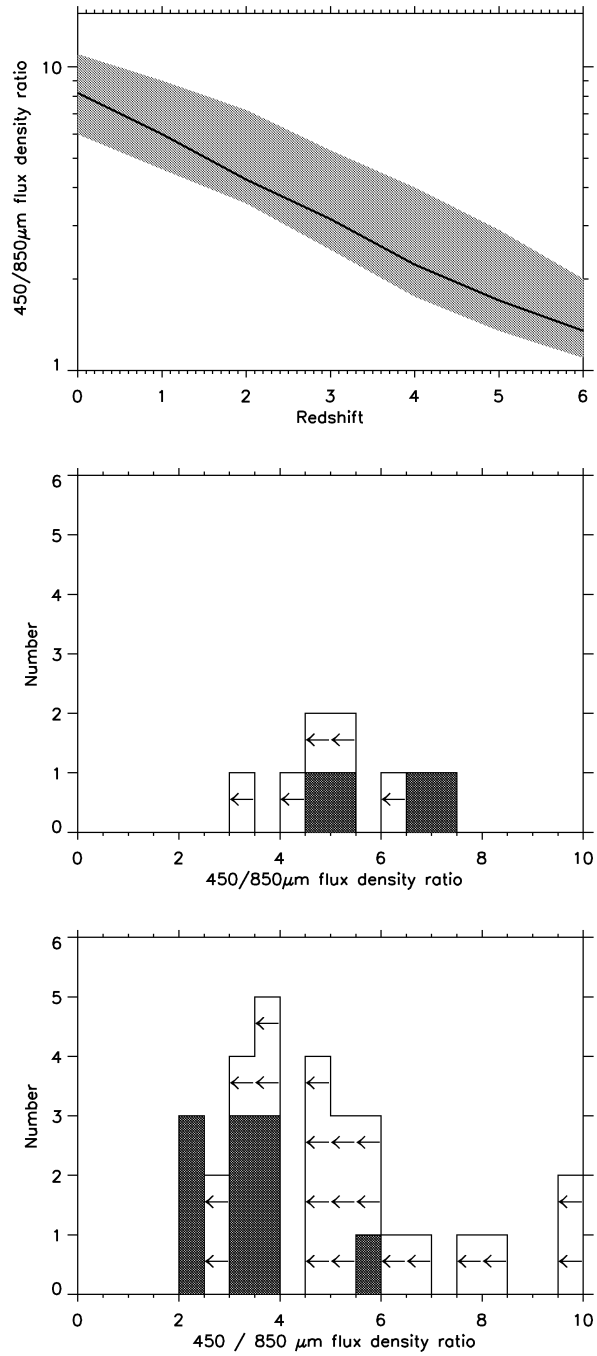

Figure 6. Top: The 450- to 850-μm flux density ratio as a function of redshift derived by Lutz et al. (2001) by redshifting the spectral energy distributions of 14 local ultra-luminous infrared galaxies (ULIRGs). The solid line displays the median relation and the shaded region shows the total scatter of the points. Middle: Histograms of the 450- to 850-μm flux density ratios for those sources detected with a significance above 4σ in the fields of the high-redshift clusters. The filled boxes represent sources detected at both wavelengths and the open boxes represent the 4σ upper limits for sources undetected at 450 μm. Only the measured ratios or limits are shown; statistical and calibration errors (which can be $\gtrsim$25 per cent) are not indicated. Bottom: A similar plot combined for sources in the blank fields of the 8-mJy survey (Scott et al. 2002; Fox et al. 2002) and the SCUBA lensing survey (Smail et al. 1997, 2002). The sources detected towards the high-redshift clusters have systematically higher 450- to 850-μm flux density ratios, consistent with being at lower redshifts ($z \sim 1$) than those found in blank field surveys (typically $z \gtrsim 2$).

$$M_{\rm d} = \frac{S(\nu_{\rm obs}) D_{\rm L}^2}{(1+z)\kappa_{\rm d}(\nu_{\rm rest}) B(\nu_{\rm rest}, T_{\rm d})},$$

where S is the observed flux density, $\nu_{\rm obs}$ and $\nu_{\rm rest}$ are the observed and rest-frame frequencies, $D_{\rm L}$ is the luminosity distance, z is the redshift, $\kappa_{\rm d}$ is the mass absorption coefficient, B is the blackbody Planck function, and $T_{\rm d}$ is the dust grain temperature. Here, a dust temperature $T_{\rm d} \sim 40$ K, and a mass absorption coefficient $\kappa_{\rm d} = 0.067(\nu_{\rm rest}/250{\rm GHz})^{\beta}$ m^2 kg^{-1} with $\beta = 2$ are adopted: for a discussion of the uncertainties on these parameters see Hughes, Dunlop & Rawlings (1997). With these properties then a source with a flux density of 10 mJy at 850 μm would have a dust mass of $\sim 5 \times 10^8$ M$_\odot$ if it were at redshift $z \sim 1$. If it is assumed that this dust is heated primarily by young stars, then scaling the submm luminosity to the star-formation rate by using nearby starbursts such as M82 (Hughes et al. 1997), the star formation rate for a 10-mJy 850 μm source at $z = 1$ is $\sim$2000 M$_\odot$ yr^{-1}. Thus any confirmed submm emitting cluster members are undergoing extremely active starbursts.

5 CONCLUSIONS

SCUBA observations have been presented of the central regions of four rich cluster of galaxies at redshifts $z \sim 1$. Compared with the number counts determined from blank-field surveys, an excess of submm sources of a factor $\sim$3–4 at 850 μm and up to an order of magnitude at 450 μm has been detected. Some fraction of this excess will be due to the effects of gravitational lensing magnification of background sources by the clusters; an analysis of possible source count boosting by gravitational lensing has been carried out and demonstrates that, unless the measured velocity dispersions greatly underestimate the cluster masses, this could boost the source counts by at most a factor of two. The residual excess counts are most likely directly associated with the high-redshift clusters. This conclusion is strengthened by the typically higher 450- to 850-μm flux density ratios of these sources as compared with blank-field selected sources. These higher ratios are consistent with a significant proportion of the sources being at lower redshifts than those of the blank field surveys (typically $z \gtrsim 2$).

Confirmation that these submm sources are indeed associated with cluster galaxies would indicate a dramatic increase with redshift in the proportion of strongly starbursting galaxies within clusters. This mirrors the increasing fraction of blue, star-forming galaxies indicated by the Butcher–Oemler effect (Butcher & Oemler 1978), and the recent discovery that more distant clusters often contain an enhanced population of weak radio sources (Dwarakanath & Owen 1999; Morrison 1999; Best et al. 2002). All of these results demonstrate that high-redshift clusters are still in a very active state of formation. With a larger data set it would be particularly interesting to investigate the radial distribution of the submm sources within the clusters, and to investigate whether mergers between clusters, which are common at these high redshifts, increase the proportion of starbursting galaxies.

ACKNOWLEDGMENTS

I would like to thank the Royal Society for generous financial support through its University Research Fellowship scheme. The JCMT is operated by the Joint Astronomy Centre on behalf of the United Kingdom Particle Physics and Astronomy Research Council (PPARC), the Netherlands Organisation for Scientific Research and the National Research Council of Canada. I thank Susie Scott for useful discussions about matters of SCUBA data reduction and Rob Ivison et al for supplying the 450-μm flux densities of the SCUBA lensing survey sample prior to publication. I particularly thank Ian Smail, Rob Ivison and Jim Dunlop for their careful reading of the manuscript and helpful comments. I am grateful to the referee for a number of suggestions which have improved the manuscript.

REFERENCES

Adelberger K. L., Steidel C. C., 2000, ApJ, 544, 218
Almaini O. et al., 2002, MNRAS, in press (astro-ph/0108400)
Archibald E. N., Wagg J. W., Jenness T., 2000, SCD System Note 2.2 (http://www.jach.hawaii.edu/JACdocs/JCMT/SCD/SN/002.2)
Archibald E. N. et al., 2002, MNRAS, in press (astro-ph/0204444)
Barger A. J., Cowie L. L., Sanders D. B., 1999, ApJ, 518, L5
Best P. N., van Dokkum P. G., Franx M., Röttgering H. J. A., 2002, MNRAS, 330, 17
Blain A. W., Longair M. S., 1993, MNRAS, 264, 509
Blain A. W., Kneib J.-P., Smail I., Ivison R. J., 1999, ApJ, 512, L87
Blandford R., Narayan R., 1992, ARA&A, 30, 311
Butcher H. R., Oemler A., 1978, ApJ, 219, 18
Carilli C. L., Yun M. S., 2000, ApJ, 530, 618
Castander F. J., Ellis R. S., Frenk C. S., Dresler A., Gunn J. E., 1994, ApJ, 424, L79
Chapman S. C. et al., 2000, MNRAS, 319, 318
Chapman S. C., Scott D., Borys C., Fahlman G. G., 2002, MNRAS, 330, 92
Cowie L. L., Barger A. J., Kneib J.-P., 2002, AJ, 123, 2197
Downes D. et al., 1999, A&A, 347, 809
Dressler A. et al., 1997, ApJ, 490, 577
Dressler A., Smail I., Poggianti B. M., Butcher H., Couch W. J., Ellis R. S., Oemler A., 1999, ApJS, 122, 51
Dunlop J. S. et al., 2002, MNRAS, submitted (astro-ph/0205480)
Dwarakanath K. S., Owen F. N., 1999, ApJ, 118, 625
Eales S. A., Lilly S., Webb T., Dunne L., Gear W., Clements D., Yun M., 2000, AJ, 120, 2244
Edge A. C., Ivison R. J., Smail I., Blain A. W., Kneib J.-P., 1999, MNRAS, 306, 599
Ellis R. S., Smail I., Dressler A., Couch W. J., Oemler A. J., Butcher H., Sharples R. M., 1997, ApJ, 483, 582
Feigelson E. D., Nelson P. I., 1985, ApJ, 293, 192
Fox M. J. et al., 2002, MNRAS, 331, 839
Gunn J. E., Gott J. R., 1972, ApJ, 176, 1
Gunn J. E., Hoessel J. G., Oke J. B., 1986, ApJ, 306, 30
Högbom J. A., 1974, A&AS, 15, 417
Holland W. S. et al., 1999, MNRAS, 303, 659
Hughes D. H., Gaztañaga E., 2000, in Favata F., Kaas A., Wilson A., eds, Proc. of 33rd ESLAB Symp., Star Formation from the Small to the Large Scale. ESA SP-445
Hughes D. H., Dunlop J. S., Rawlings S., 1997, MNRAS, 289, 766
Hughes D. H. et al., 1998, Nat, 394, 241
Ivison R. J., Dunlop J. S., Smail I., Dey A., Liu M. C., Graham J. R., 2000a, ApJ, 542, 27
Ivison R. J., Smail I., Barger A. J., Kneib J.-P., Blain A. W., Owen F. N., Kerr T. H., Cowie L. L., 2000b, MNRAS, 315, 209
Jenness T., Lightfoot J. F., 1998, in Albrecht R., Hook R. N., Bushouse H. A., eds, ASP Conf. Ser. Vol 145, Astronomical Data Analysis Software and Systems VII. Astron. Soc. Pac., San Francisco, p. 216
Klaas U. et al., 2001, A&A, 379, 823
LaValley M., Isobe T., Feigelson E., 1992, BAAS, 24, 839
Lubin L. M., Brunner R., Metzger M. R., Postman M., Oke J. B., 2000, ApJ, 531, L5
Lutz D. et al., 2001, A&A, 378, 70
Madau P., Pozzetti L., Dickinson M., 1998, ApJ, 498, 106
Morrison G. E., 1999, PhD thesis, Univ. New Mexico
Navarro J. F., Frenk C. S., White S. D. M., 1997, ApJ, 490, 493
Oke J. B., Postman M., Lubin L. M., 1998, AJ, 116, 549
Peacock J. A. et al., 2000, MNRAS, 318, 535

Postman M., Lubin L. M., Oke J. B., 1998, AJ, 116, 560
Postman M., Lubin L. M., Oke J. B., 2001, AJ, 122, 1125
Rosati P., Stanford S. A., Eisenhardt P. R., Elston R., Spinrad H., Stern D., Dey A., 1999, AJ, 118, 76
Schade D., Barrientos L. F., Lopez-Cruz O., 1997, ApJ, 477, L17
Scott S. E. et al., 2002, MNRAS, 331, 817
Smail I., Ellis R. S., Fitchett M. J., 1994, MNRAS, 270, 245
Smail I., Ivison R. J., Blain A. W., 1997, ApJ, 490, L5
Smail I., Morrison G., Gray M. E., Owen F. N., Ivison R. J., Kneib J.-P., Ellis R. S., 1999, ApJ, 525, 609
Smail I., Ivison R. J., Owen F. N., Blain A. W., Kneib J.-P., 2000, ApJ, 528, 612
Smail I., Ivison R. J., Blain A. W., Kneib J.-P., 2002, MNRAS, 331, 495
Stanford S. A., Eisenhardt P. R., Dickinson M., 1998, ApJ, 492, 461
Stanford S. A., Elston R., Eisenhardt P. R., Spinrad H., Stern D., Dey A., 1997, AJ, 114, 2232
Steidel C. C., Giavalisco M., Pettini M., Dickinson M., Adelberger K. L., 1996, ApJ, 462, L17
van Dokkum P. G., Franx M., Kelson D. D., Illingworth G. D., 1998a, ApJ, 504, L17
van Dokkum P. G., Franx M., Kelson D. D., Illingworth G. D., Fisher D., Fabricant D., 1998b, ApJ, 500, 714
van Dokkum P. G., Franx M., Fabricant D., Kelson D. D., Illingworth G. D., 1999, ApJ, 520, L95

This paper has been typeset from a TEX/LATEX file prepared by the author.